Adverse-pressure-gradient turbulent boundary layer on convex wall

Saurabh Pargal,[1,2] Hao Wu (吴昊),[2,3] Junlin Yuan (袁隽琳),[1] and Stéphane Moreau[2]

[1)]*Department of Mechanical Engineering, Michigan State University, East Lansing, MI 48823, USA*

[2)]*Department of Mechanical Engineering, Université de Sherbrooke, Sherbrooke, Quebec J1K 2R1, Canada*

[3)]*Department of Plasma Research, General Fusion, Burnaby, British Columbia, V3N 4T5, Canada*

(*Electronic mail: pargalsa@msu.edu)

Direct numerical simulations (DNS) of an incompressible turbulent boundary layer on an airfoil (suction side) and that on a flat plate are compared to characterize the non-equilibrium turbulence and the effect of wall curvature on the flow. The two simulations effectively impose matching streamwise distributions of adverse pressure gradient (APG) quantified by the acceleration parameter (K). For the airfoil flow, an existing compressible DNS carried out by Wu, Moreau and Sandberg, *J. Fluid Mech.*, **868**, 584–610 (2019) of the flow around a controlled-diffusion airfoil is used. For the flat-plate flow, a separate simulation is carried out with the aim to reproduce the flow in the region of the airfoil boundary layer with zero to adverse pressure gradients. Comparison between the two cases extracts the effect of a mild convex wall curvature on velocity and wall-pressure statistics in the presence of APG. In the majority part of the boundary layer development, curvature effect on the flow is masked by that of the APG, except for the region with weak pressure gradients or a thick boundary layer where the effect of wall curvature appears to interact with that of APG. High-frequency wall-pressure fluctuations are also augmented by the wall curvature. Overall, the boundary layers are qualitatively similar with and without the wall curvature. This indicates that a flat-plate boundary layer DNS may serve as a low-cost surrogate of a boundary layer over airfoil or other objects with mild curvatures to capture important flow features to aid modeling efforts.

I. INTRODUCTION

Turbulent boundary layer flows are ubiquitous. Existing physical understandings and models of wall-bounded turbulent flows are usually focused on equilibrium flows such as fully developed channels and turbulent boundary layers with statistics that are invariant along the streamwise direction[1]. Yet, most flows encountered in realistic applications are non-equilibrium flows, such as those characterized by unsteadiness and streamwise varying pressure gradients that are induced by curvature of the wall. Existing turbulence models often yield significant uncertainties in predicting flows with large departure from the equilibrium state[2–7].

This work focuses on a type of boundary layers developed on surfaces with mild curvatures, such as airfoils in low-speed fan applications. We focus on a subset of non-equilibrium boundary layers—those with streamwise varying adverse pressure gradient and convex wall curvature. Typically, the pressure gradients experienced by the boundary layer is generated by the wall curvature. The strength of a pressure gradient can be quantified by the Clauser parameter[8,9], $\beta(x) = (\delta^*/\tau_w)(\mathrm{d}P_\infty/\mathrm{d}x)$, where δ^* is the displacement thickness, τ_w is the wall shear stress, $\mathrm{d}P_\infty/\mathrm{d}x$ is the freestream pressure gradient and x is streamwise coordinate. For a non-equilibrium boundary layer, β varies along the flow direction. Another dimensionless pressure gradient often used is the acceleration parameter, $K(x) = (\nu/U_\infty^2)(\mathrm{d}U_\infty/\mathrm{d}x)$, where ν is the kinematic viscosity, and U_∞ is the streamwise freestream velocity.

The effects of APG on the boundary layer have been widely studied theoretically, experimentally and numerically in the past decades[10–26]. The consensus is that APG leads to reduced wall friction compared to that in a zero-pressure-gradient (ZPG) boundary layer, an increase in the outer peak of Reynolds stresses due to excitation of large turbulent structures in the outer layer, a stronger wake in the mean velocity profile, and augmented sweep events. Na and Moin [14,15] investigated effects of pressure gradient on turbulent boundary layer with and without separation using DNS. They found that in addition to the aforementioned effects of APG, the two-point correlation of wall-pressure fluctuations is widened in the spanwise direction, and vice-versa in the case of favourable pressure gradients (FPG). Moreover, the convection velocity of wall-pressure fluctuations, defined based on the space-time correlation of the pressure fluctuations, is extensively reduced in the presence of APG. Based on laser doppler anemometer measured statistics of a non-equilibirum APG boundary layer, Aubertine and Eaton [19] pointed out that even with mild pressure gradients (with β from 0 to 2), the boundary layer is non-equilibrium. Harun *et al.* [12] carried out experiments to understand the effect of pressure gradients. They showed that the large-scale structures across the boundary layer are more energized in APG boundary layers compared to those with ZPG. Kitsios *et al.* [17,18] studied equilibrium boundary layers with ZPG, mild APG (with $\beta = 1$) or strong APG on the verge of separation (with $\beta = 39$) based on DNS. They found that in APG boundary layers the Reynolds stresses, turbulence production and dissipation rate all exhibit an outer-layer peak. Lee and Sung [27] evaluated the effect of APG on turbulent structures, and found that under APG, the average spacing of near-wall streaks is increased and the outer region of the boundary layer is filled with streamwise aligned vortex packets. Monty, Harun, and Marusic [22] carried out parametric studies for APG boundary layers based on measurements using hot-wire anemometry and found that, under approximately the same β values, turbulent statistics do not vary significantly even with different Reynolds numbers. But with different β values, turbulent statistics vary even with similar Reynolds numbers and acceleration parameters, K.

The Boundary layer flow statistics are not only affected by the local $\beta(x)$ value, but also its accumulated history prior to that location. This is termed the "history effect" of the pressure gradient[20,21,23,24,28]. Based

on large-eddy simulations (LES) and DNS data on flat plate and airfoils, Bobke *et al.* [20] and Vinuesa *et al.* [24] studied the history effect of β. They showed that, even with matched local β values, turbulent statistics between boundary layers can be different, dependent on the flow development prior to that location and the streamwise variation of β. This also helps explain boundary layer development on airfoils, as studied by Vinuesa *et al.* [26,29].

The effects of longitudinal convex wall curvature on turbulent boundary layers have already been studied[19,30–41]. Bradshaw [30,31] showed that even a mild convex curvature weakens turbulent diffusion to the outer layer. Ramaprian and Shivaprasad [32] showed that a mild convex curvature reduces the Reynolds stresses in the outer layer and enhances turbulent kinetic energy distribution to smaller scales. So and Mellor [36] carried out experiments with strong convex curvatures; they found that the Reynolds stresses decrease both near the wall and in the outer layers. Gillis and Johnston [34] conducted experiments at medium and strong convex curvatures; they showed that normalizing the wall-normal distance using the radius of curvature (R) collapses the wall-normal Reynolds shear stress profiles. Established understanding of the effects was summarized by Patel and Sotiropoulos [38]: with a stronger convex curvature, there is considerable reduction in Reynolds stresses especially in the outer region, a decrease in skin friction, increase in the wake in of mean velocity profile, and reduction in turbulent diffusion to the outer layer. Most of these existing studies aimed to understand the sensitivity of boundary layers to longitudinal convex curvatures, free of the interference of any pressure gradient. Thus the pressure gradients were kept minimal in these studies.

II. OBJECTIVES

The objective of the present work is to understand the effect of convex curvature in the presence of APG that is relevant to low-speed fan applications[42,43] (with Reynolds numbers based on the chord length below 10^6) and other applications with radii of surface curvature higher than around 50 times of the local boundary layer thickness, such as a highly cambered airfoil close to its separation point in a turbomachinery. The purpose is two-fold: one is to enrich the fundamental understanding of non-equilibrium turbulent boundary layers on a curved wall, which is present in many engineering applications; the other is to gauge the suitability of using flat-plate simulations on individual sides of the airfoil as low cost surrogates of airfoil-flow simulations for DNS data collection to aid turbulence and aeroacoustics model[44–52] development. To this end, DNS simulations of flow over the suction side of a controlled-diffusion (CD) airfoil[53] and flow over a flat plate are compared. Both flows are subjected to matching streamwise pressure gradient quantified by the acceleration parameter, K. Comparison between the two cases isolates the effect of wall curvature.

The organization of the paper is as follows. The governing equations, numerical methods, parameters and solver validation are described in Sec. III. Section IV presents results of the comparison on boundary layer development and flow statistics (Sec. IV A to Sec. IV C), as well as characteristics of wall-pressure fluctuations (Sec. IV D). Conclusions are provided in Sec. V.

III. APPROACH

Data on the CD airfoil flow are available from Wu, Moreau, and Sandberg [53,54]. The distribution of $K(x)$ of the boundary layer on the suction side is shown in Fig. 1(a). Along the streamwise direction, the boundary layer

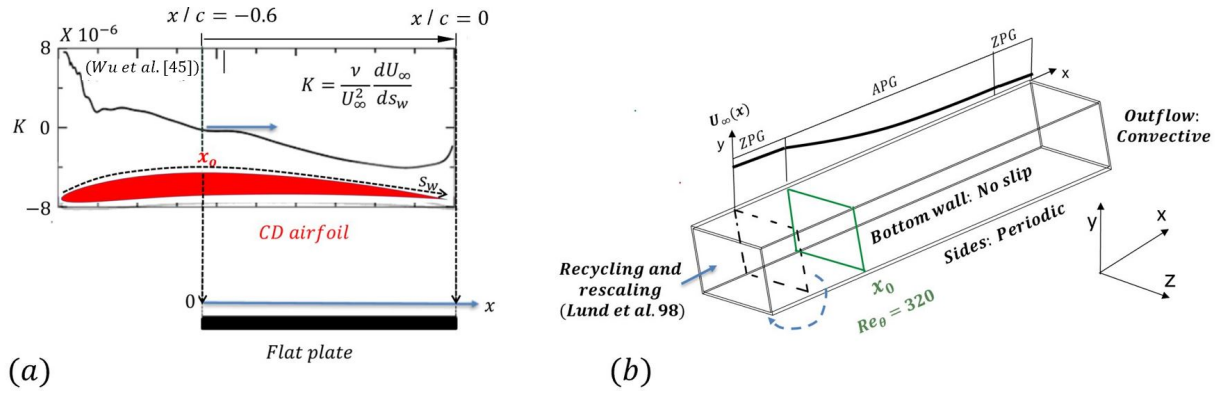

图 1. (a) Sketch of the useful streamwise domain of the flat-plate DNS designed to match $K(x)$ of the airfoil boundary layer from $x/c = -0.6$ downstream. (b) Simulation domain and boundary conditions used in the flat-plate simulation.

first experiences FPG ($K > 0$), then ZPG ($K \approx 0$) near the mid-chord location and APG ($K < 0$) downstream. A separate DNS of a flat-plate boundary layer is conducted and is described in this section. The simulation is designed to match the $K(x)$ distribution of the airfoil flow in the ZPG to APG region only (i.e. from around mid-chord, $x/c = -0.6$, to the trailing edge $x/c = 0$, where c is the airfoil chord length). In the flat-plate simulation, an x axis different from that in the airfoil simulation is used. The start of the useful region (x_o) of the flat-plate simulation corresponds to $x/c = -0.6$ location on the airfoil, as shown in Fig 1(a).

The incompressible flow of a Newtonian fluid is governed by the equations of conservation of mass and momentum:

$$\frac{\partial u_i}{\partial x_i} = 0, \tag{1}$$

$$\frac{\partial u_j}{\partial t} + \frac{\partial u_i u_j}{\partial x_i} = -\frac{\partial P}{\partial x_j} + \nu \frac{\partial^2 u_j}{\partial x_i \partial x_i}. \tag{2}$$

Here, x_1, x_2 and x_3 (or x, y and z) are, respectively, the streamwise, wall-normal and spanwise directions, u_1, u_2 and u_3 (or u, v and w) are the velocity components in those directions, t is time, $P = p/\rho$ is the modified pressure, ρ is the density and ν is the kinematic viscosity. The flat-plate simulation is performed using a well-validated code that solves the governing equations (1) and (2) on a staggered grid using second-order, central differences for all spatial derivatives, second-order accurate Adams-Bashforth semi-implicit time advancement, and MPI parallelization[55]. An instantaneous flow variable $\phi(x,y,z,t)$ is decomposed as $\phi = \langle\overline{\phi}\rangle(x,y) + \phi'(x,y,z,t)$, where $\langle\cdot\rangle$ denotes spatial averaging in z and $\overline{(\cdot)}$ denotes averaging in time.

For the flat-plate DNS, the freestream pressure gradient is imposed by prescribing the streamwise-varying $U_\infty(x)$ at the top boundary of the domain (indicated in Fig. 1(b)); the wall-normal freestream velocity $V_\infty(x)$ is obtained based on the conservation of mass[56]. A fully turbulent boundary layer flow upstream of the useful domain is obtained using the recycling/rescaling method of Lund, Wu, and Squires[57]. A convective outflow boundary condition[58] is used at the outlet and periodic boundary conditions are used in the spanwise direction.

The domain sizes in x, y and z are $930\,\theta_o$, $100\,\theta_o$ and $80\,\theta_o$, respectively. Here, $\theta(x) = \int_0^\delta U(x,y)[U_\infty(x) - U(x,y)]\mathrm{d}y/U_\infty(x)^2$ is the momentum thickness and θ_o is the θ value at the x_o location. δ is calculated based on the total pressure method[43,53,59]. Specifically, the wall-normal profile of mean total pressure at each streamwise location, $P_t(x,y) = 0.5\rho U(x,y)^2 + P_s(x,y)$ (where P_t is the total pressure, P_s is the mean static pressure, and

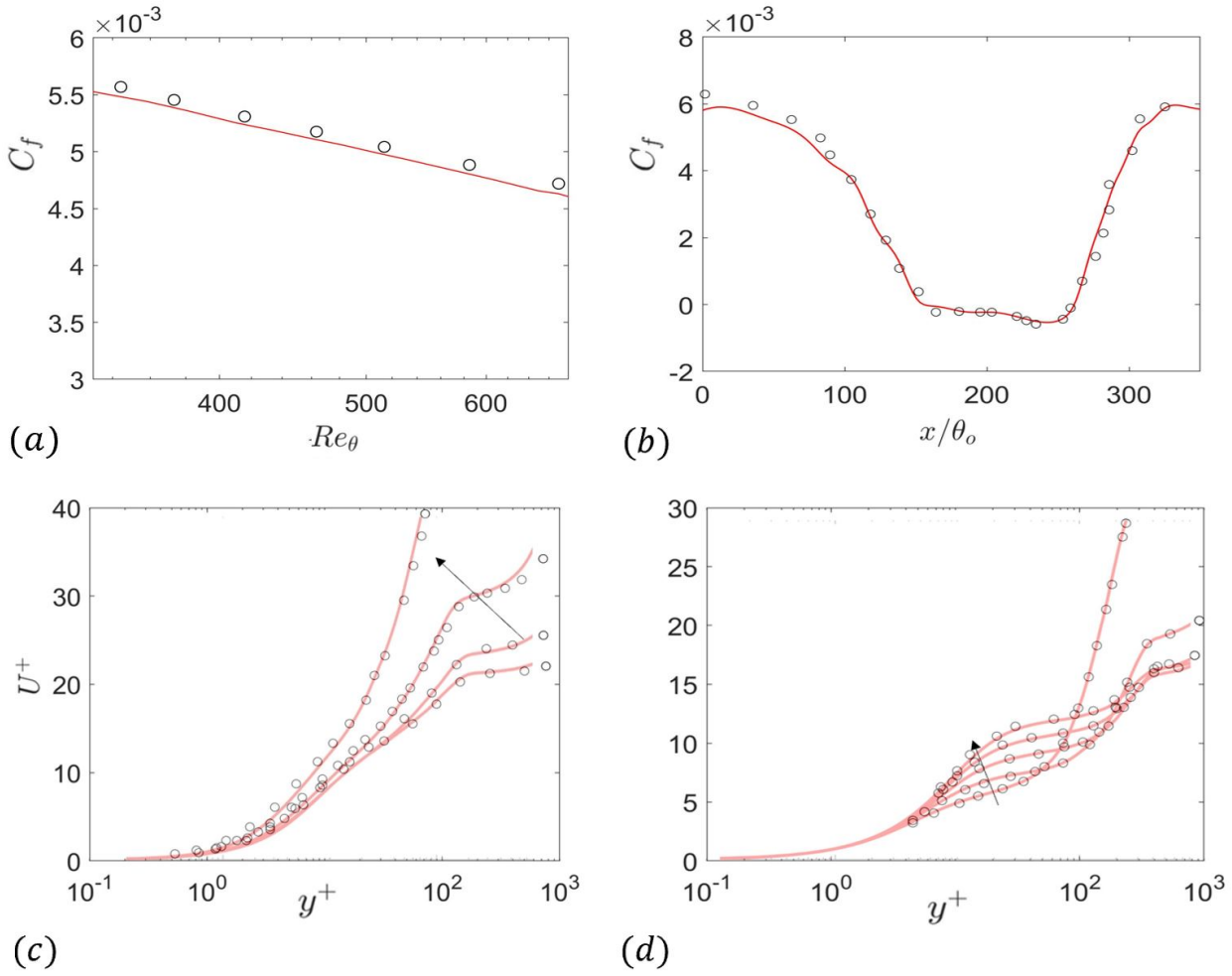

图 2. Validation of boundary layer simulations. (a) Skin friction coefficient comparison between present test case (——) and ZPG boundary layer DNS of Schlatter and Örlü [60] (○); (b) Skin friction comparison between present test case (——) and APG boundary layer DNS data of Na and Moin [14] (○). (c,d) Comparisons of streamwise mean velocity (——) with Na and Moin[14] (○): (c) before detachment ($x/\delta^* = 100$, 115, 130 and 145 in arrow direction) and (d) after reattachment ($x/\delta^* = 270$, 285, 300 and 330 in arrow direction).

$U \equiv \langle \overline{u} \rangle$) is calculated; the wall-normal location at which P_t reaches 95% of its maximum value is defined as the edge of the boundary layer. The streamwise length of the recycling/rescaling region is $75\,\theta_o$. The x_o is located at $150\,\theta_o$ downstream from the most upstream location of the domain. The pressure gradient is applied starting from x_o for $400\,\theta_o$ downstream, up to the corresponding trailing-edge location of the airfoil. Uniform grids are used in x and z, while in y the grid is refined near the wall. The x and z grid sizes in wall units are $\Delta x^+ \in [4, 10]$ and $\Delta z^+ \in [2, 5]$. In y, the smallest grid size (at the wall) for each x is $\Delta y^+_{\text{min}} \in [0.06, 0.15]$. The u' two-point correlation at a spanwise separation of half the spanwise domain size is less than 0.1, indicating that the spanwise domain size is sufficiently large. The total number of grid points are 1536, 200 and 256 in x, y and z directions, respectively. The total averaging time for simulation is $T \approx 3000\theta_o/U_o$. The Reynolds numbers based on the momentum thickness (Re_θ) at the x_o locations are 320 in both cases.

The fluid solver was validated by running a ZPG flat-plate boundary layer simulation and comparing it with

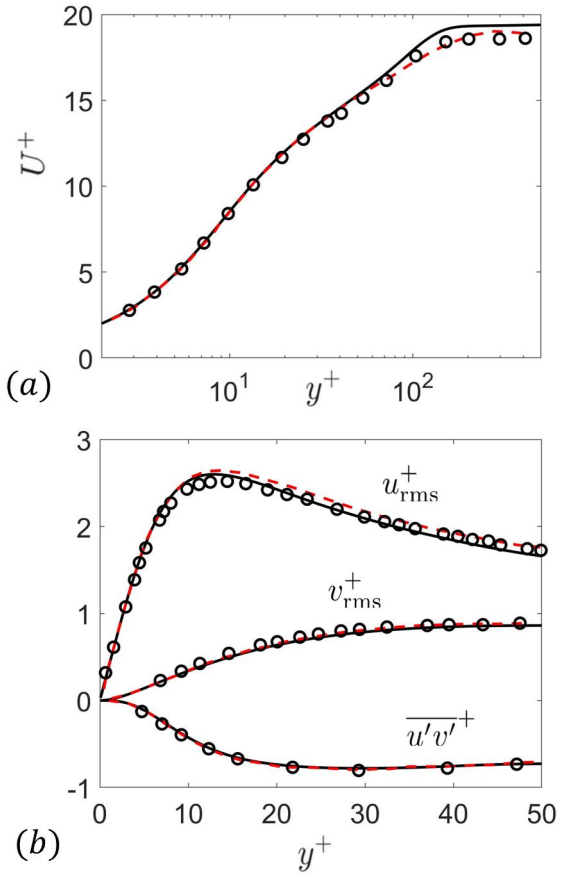

图 3. Comparison between airfoil (– – –) and flat-plate cases (———) at the inlet of the boundary layer flow (or $x/c = -0.6$ location on the airfoil): (a) streamwise mean velocity and (b) Reynolds stresses normalized by inner units. ∘ Spalart[61] data at a similar Re_θ.

the results of Schlatter and Örlü[60] with similar Reynolds numbers. The comparison of skin friction $C_f(x) = 2\tau_w/\rho U_\infty^2$ shows excellent agreement in Fig. 2(a). To validate the prescription of the mean pressure gradient at the top boundary, another DNS was carried out to reproduce the results of a separating boundary-layer flow conducted by Na and Moin[14]. Very good agreement in C_f is shown in Fig. 2(b), and in the mean velocity profiles before and after the boundary layer separation, as shown in Figs. 2(c) and (d) respectively.

IV. RESULTS

A. Statistics at the inlet of flat-plate boundary layer

From here on, the x_o location at the airfoil is set as $x = 0$ (and called the "inlet") for the flat-plate simulation. Before comparing the developments of the flat-plate boundary layers and the airfoil one in the APG region, the extent to which the flat-plate boundary layer inlet represents the airfoil boundary at $x/c = -0.6$ is evaluated in this section. Both single-point and two-point statistics are compared between the flow at $x = 0$ for the flat-plate boundary layer and the flow at $x/c = -0.6$ for the airfoil boundary layer.

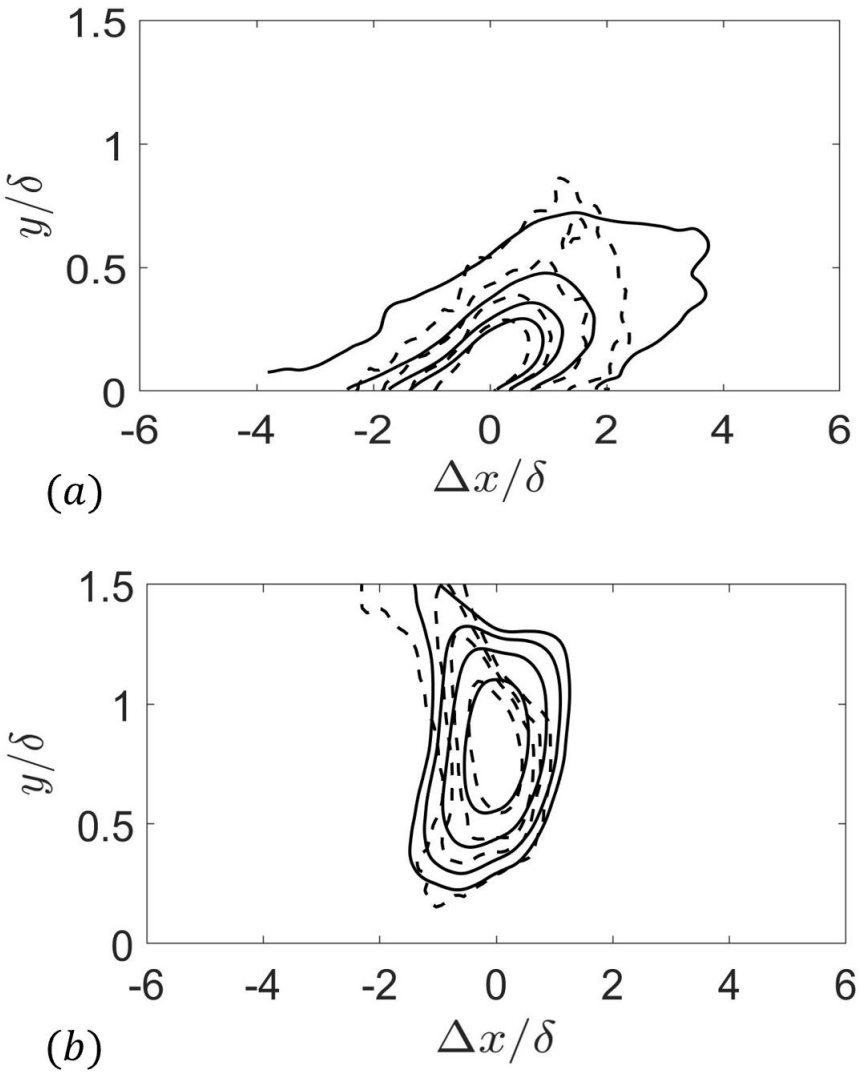

图 4. Comparison (at x_o) of two-point correlations of u' in x-y plane centered at (a) $y/\delta = 0.1$ and (b) $y/\delta = 0.8$, at the inlet of the boundary layer flow: ——— airfoil case; - - - flat-plate case. Contour levels are 0.05, 0.15, 0.25, and 0.35.

In Fig. 3, the comparisons of the streamwise mean velocity and the Reynolds stresses are shown, together with the results of a ZPG boundary layer simulation by Spalart[61] at a similar Reynolds number of $Re_\theta \approx 300$. The profiles of all cases match very well. The mean velocity profile in the airfoil simulation is slightly lower in the outer region, which is probably due to the FPG imposed upstream of this x location because of the airfoil curvature. The friction coefficient is approximately 5 percent higher in the airfoil case, consistent with the difference in the U_∞^+ value shown in Fig. 3(a). For the root-mean-square (r.m.s.) velocities and Reynolds shear stress, the differences between the three cases are within 5 percent.

Next, the structural characteristics of the two cases are compared using two point velocity correlations, R_{uu}, which is defined as

$$R_{uu}(r_x, r_y, y_{\text{ref}}) = \langle \overline{u'(x, y_{\text{ref}}, z, t) u'(x + r_x, y_{\text{ref}} + r_y, z, t)} \rangle / \langle \overline{u'^2} \rangle (y_{\text{ref}}), \tag{3}$$

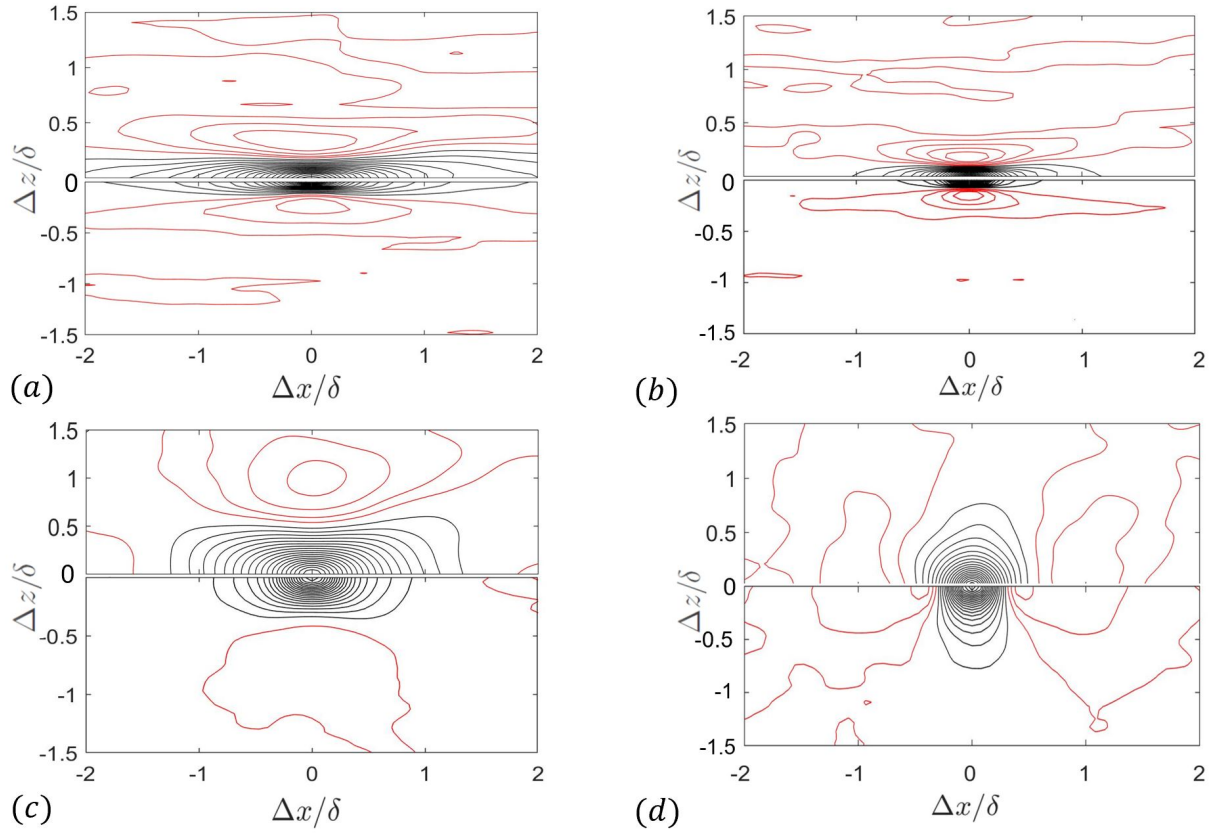

图 5. Comparison (at x_o) of two-point correlations of (a,c) u' and (b,d) v' in x-z plane at (a,b) $y/\delta = 0.1$ and (c,d) $y/\delta = 0.8$ for airfoil (top half) and flat-plate (bottom half) cases. ——— Positive contour levels from 0.05 to 0.9 with a step size of 0.05; ——— negative contour levels of -0.01,-0.05, -0.1 and -0.15.

where r_{x_i} is the separation in x_i direction and y_{ref} is the elevation at which the correlation is centered. In Figs. 4 and 5, the two-point correlations of u' and v' in x-y and x-z planes are compared, centered near ($y/\delta = 0.1$) and away ($y/\delta = 0.8$) from the wall.

First, the x-y contour lines of the auto-correlations of u' centered at a near-wall and an outer elevations are shown in Figs. 4(a) and (b) respectively. In Fig. 4(a), the spatial extent and shape of the contour lines represent the size and shape of the coherent structures of u'. These characteristics agree well across the cases. At a low correlation level of 0.05, the overall length of structures vary between 6 to 8δ for all cases. But at correlation levels higher than 0.15, all of the cases lie in close proximity. The correlation centered at $y = 0.8\delta$ (Fig. 4(b)) shows velocity correlation across the boundary layer. Some differences are observed in correlations outside boundary layer (in the region $y/\delta > 1$), which could be due to the difference in the top boundary condition between the two cases.

The correlations of u' and v' in the x-z plane at $y = 0.1\delta$ and 0.8δ are shown next in Fig. 5. The region of positive auto-correlation of u' shows the extents in x and z of near-wall low-speed streaks. The extent is larger on the airfoil than on the flat plate, which is due to the FPG region in the airfoil boundary layer prior to $x/c = -0.6$. It is known that FPG stabilizes near-wall coherent motions associated with a lower bursting frequency and, consequently, leads to elongated near-wall streaks[21,56,62,63]. Similar observations are made for

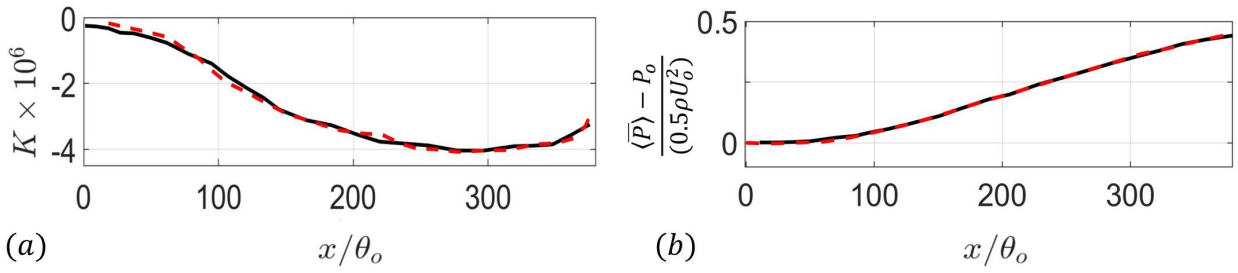

图 6. Developments of the acceleration parameter (a) and the mean wall pressure (b) along the stream-wise direction: ——— flat-plate case, - - - airfoil case. P_o and U_o are the mean wall pressure and free stream velocity at x_o location.

the v' auto-correlation. These results are overall consistent with the observations made by Sillero, Jiménez, and Moser[64] for a flat-plate ZPG boundary layer with Re_θ ranging from 2780 to 6680, indicating that velocity correlations are weakly sensitive to the Reynolds number.

These results demonstrate that the boundary layer over the airfoil is fully turbulent at $x/c = -0.6$, after the laminar separation bubble at the leading edge and the subsequent transition to turbulence. The comparison also provides confidence that the inlet state of the flat-plate flow essentially matches that in the airfoil boundary layer at $x/c = -0.6$. The developments of the two boundary layers from this streamwise location downstream are compared in the next section.

B. Boundary layer development

Figure 6(a) shows the distributions of the acceleration parameter $K(x)$ that are designed to match between the two cases. Note that $K(x)$ is calculated at the edge of the boundary layer, $y/\delta(x) = 1$. The streamwise variations of the mean pressure at the wall in the two cases also match very well, as shown in Fig. 6(b). This justifies the setup of the present comparison; any significant difference in the boundary layer development between the two cases would be a result of the additional wall curvature in the airfoil case.

First, the streamwise variations of the strengths of wall curvature and APG are evaluated. The strength of wall curvature can be quantified by the ratio between the boundary layer thickness and the radius of curvature; it is shown in Fig. 7(a). The increasing δ/R along x toward the trailing edge indicates that curvature effects are strengthened along the streamwise direction[30,34,35,38]; this is predominantly due to the growth of the boundary layer. The δ/R ratios in the airfoil case fall in the range from small[30,31] to mild[32,33] values ($\delta/R < 0.05$) as discussed in Patel and Sotiropoulos[38].

Next, the Clauser parameter (Fig. 7(b)) shows an increase along x in both cases. As β is obtained as the pressure gradient normalized using u_τ, an increase of $\beta(x)$ along x suggests that the mean pressure force relative to near-wall forces becomes stronger with increasing x. The β values are similar between the two cases throughout most part of the boundary layer. Near the trailing edge, however, β is higher in the airfoil case, despite matching $K(x)$ and wall-pressure gradient between the two cases; this is due to the lower wall friction in the airfoil case near the trailing edge as discussed next.

The displacement thickness normalized by the momentum thickness at the inlet, $\delta^*(x)/\theta_o$, and the wall friction coefficient are compared in Figs. 7(c) and 7(d), respectively. The overall variation of $\delta^*(x)$ matches

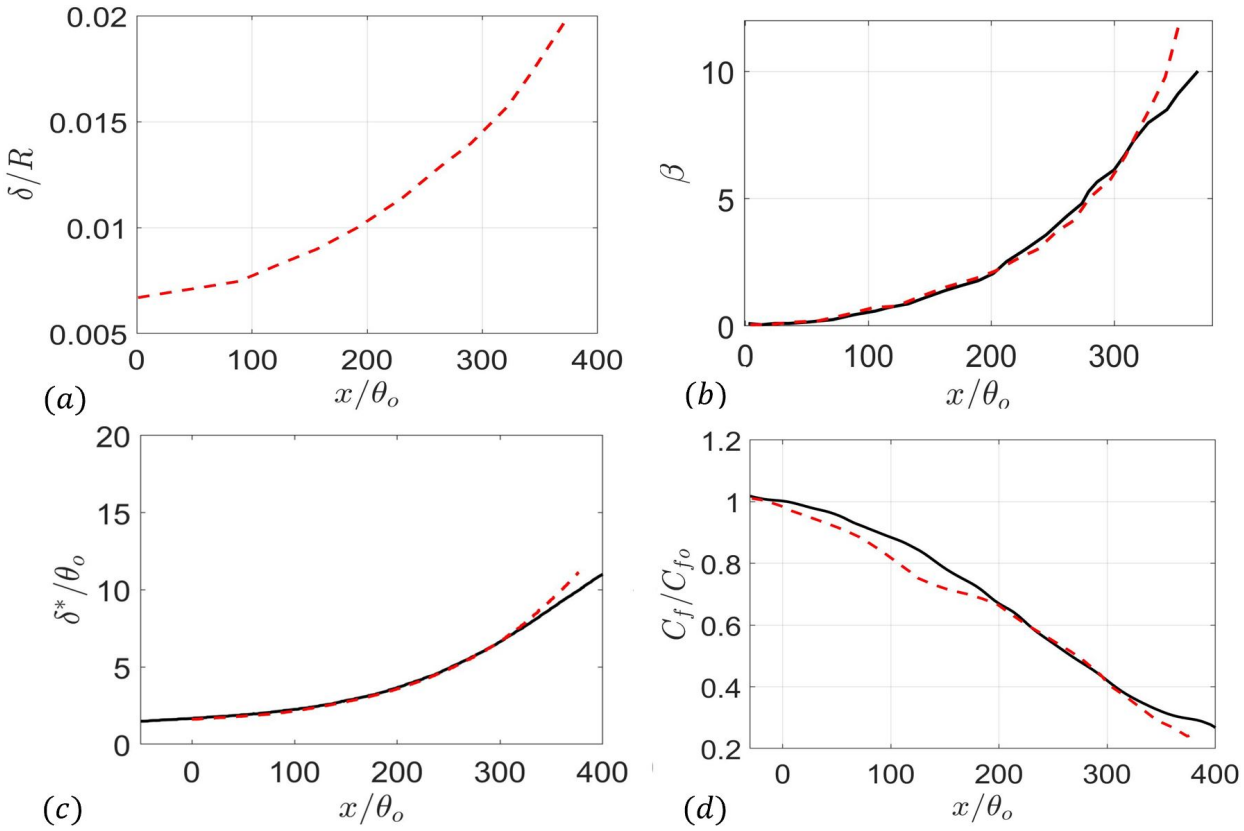

图 7. Streamwise developments of the ratio between boundary layer thickness and radius of curvature (a), Clauser parameter (b), displacement thickness (c), and skin friction coefficient normalized by its value at x_0 (d), for the airfoil (- - -) and flat-plate (——) cases.

well between the two cases, except for the region near the trailing edge where it increases faster in the airfoil case, which is most likely an APG effect due to the augmented β values along x. The comparison of $C_f(x)$ normalized by their respective values at x_o shows a faster reduction of wall friction in the airfoil flow than the flat-plate one in two regions: $x/\theta_0 < 150$ (where $\beta < 1$, i.e., weak-APG region) and $x/\theta_0 > 290$ (where $\beta > 6$, i.e., strong-APG region). In the weak-APG region, the lower C_f in the airfoil case is probably a manifestation of the effect of wall curvature observed in the past for ZPG flows [30,34,35,38]. In the strong-APG region near the trailing edge the lower C_f in the airfoil case may be due to the strengthened curvature effect (i.e., high δ/R ratio) in this region with a thickened boundary layer. The higher displacement thickness and lower C_f in the airfoil trailing edge region compared to the flat-plate case may also be due to the abrupt change in boundary conditions at the trailing edge and the airfoil wake generation downstream[65], affecting boundary layer growth immediately upstream of the trailing edge. Yet, for most part the flow δ^* and C_f are similar between the two cases.

C. Mean streamwise velocity and turbulent statistics

Figure 8 compares wall-normal profiles of the streamwise mean velocity and turbulent statistics at different stations along the streamwise direction. These locations are marked alongside the streamwise variation of β in

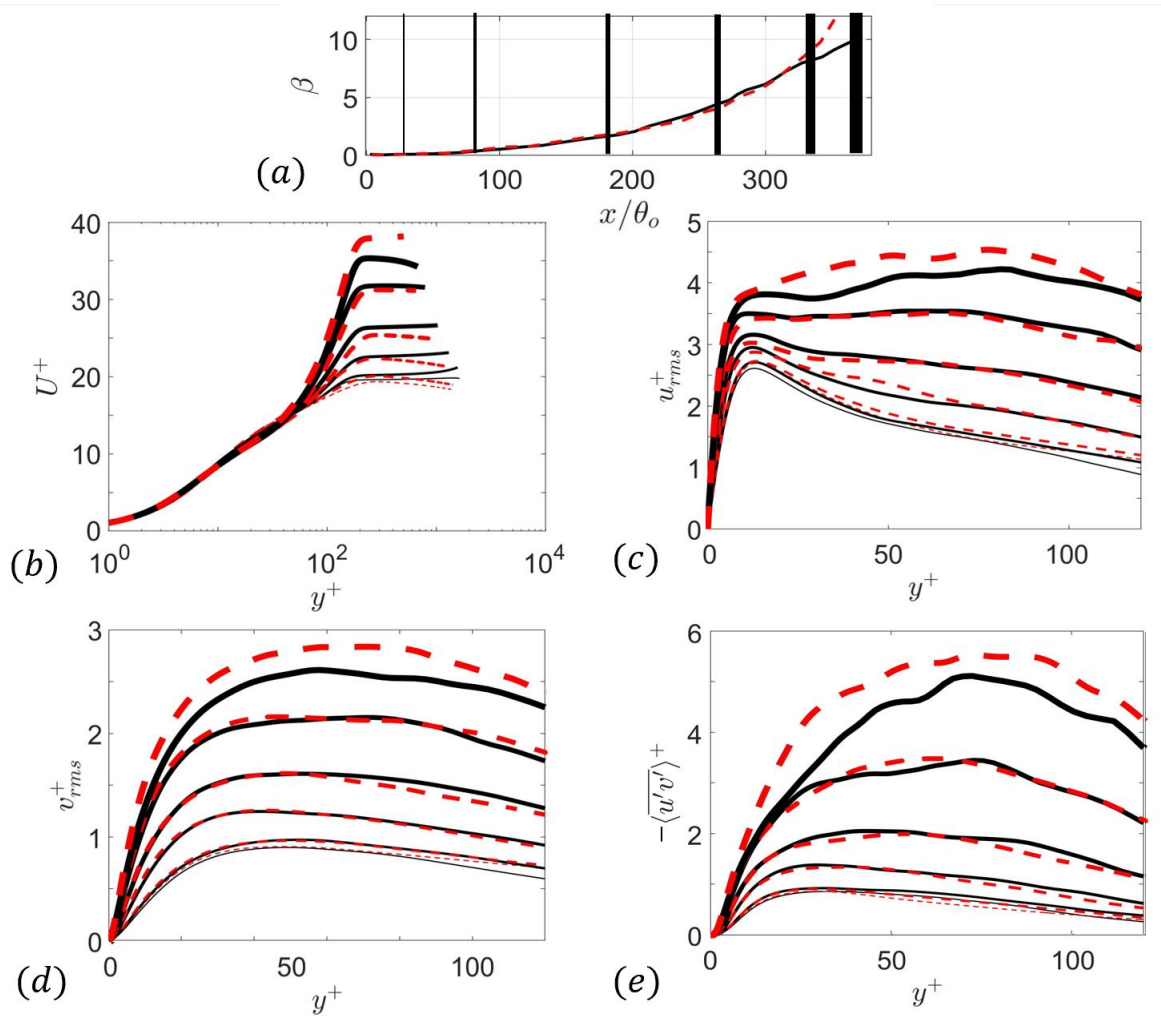

图 8. Variation of (a) Clauser parameter showing streamwise locations at which comparisons are made. Flow statistics comparisons between the airfoil (- - -) and flat-plate (———) cases at these locations: (b) velocity profile, (c) streamwise r.m.s. velocity, (d) wall-normal r.m.s. velocity, and (e) Reynolds shear stress, all normalized in wall units. Comparison is shown at five streamwise locations: $x/\theta_o = 25$, 75, 175, 250, 325, and 350, represented by lines with increasing thickness.

Fig. 8(a). The flow statistics are normalized by u_τ. The variations of the mean velocities (Fig. 8(b)) and Reynolds stresses (Fig. 8(c,d,e)) are overall similar throughout the boundary layer development between the two cases. Specifically, the wake of the mean velocity becomes intensified due to the imposed APG. The Reynolds stresses normalized by u_τ are augmented throughout the boundary layer, associated with the decrease of wall friction. For the r.m.s. velocity u_{rms}, a prominent outer peak appears at the most downstream station due to the strong APG. The augmentations of the r.m.s. velocity v_{rms} and the Reynolds shear stress in the outer layer are also evident.

The blue overall agreement between the profiles in both cases up to around $x/\theta_o = 325$ suggests that for the majority part of the flow the curvature effect (though increasingly strengthened as the boundary layer develops) is masked by the APG effect without significant modification of turbulence statistics. the low-APG region ($x/\theta_o < 175$), A slightly lower outer-layer Reynolds shear stress magnitude is observed in the airfoil case than in the flat-plate case as shown in Fig. 8(e). This is consistent with previously observed effect of curvature in

ZPG flows[19,30–41]. The main differences between the two cases are seen in the strong APG region at $x/\theta_o = 350$. Specifically, the airfoil case yields a noticeably stronger velocity wake, as well as higher outer-layer turbulence intensities and Reynolds shear stress magnitude, compared to the flat-plate case. These phenomena suggest an effectively stronger APG present in the airfoil flow, consistent with the higher β at $x/\theta_o = 350$ than in the flat-plate case as shown in Fig 8(a). It is therefore inferred that β is more appropriate than K as an indicator for the extent to which the turbulence statistics are affected by freestream pressure gradients.

These results above indicate that the airfoil boundary layer is overall similar to a flat-plate boundary layer subjected to the same pressure gradients. The increased airfoil curvature or trailing edge effects[65] for $x/\theta_o > 300$, appears to quantitatively modify the boundary layer turbulence statistics by modulating β.

D. Wall-pressure statistics

In aeroacoustics models used to predict far-field noise generated by the flow past an airfoil, the wall-pressure statistics (such as the power spectral density (PSD) and the streamwise and spanwise correlations of wall-pressure fluctuations) provide the main input parameters to predict far-field noise generated by the boundary layer. In this section, wall-pressure statistics between the airfoil and flat-plate cases are compared to pinpoint the curvature effects on wall-pressure statistics.

Figure 9(a) compares the streamwise variation of the wall-pressure r.m.s. An overall match is seen between the cases till $x/\theta_o \approx 300$. Further downstream, more intense wall-pressure fluctuations are observed for the airfoil case, again consistent with the effect of an effectively stronger APG[15,66,67].

The power spectral densities of wall-pressure fluctuations, Φ_{PP}, are calculated using fast Fourier transform with the Welch periodogram technique and Hanning window with zero padding, at three streamwise locations of the flat-plate case: $x/\theta_o = 0$, 290 and 340. These x locations correspond to the following sensor locations in the airfoil case[53], respectively: sensor 7 (in the ZPG region) and sensors 21 and 24 (both in the APG region). Figure 9(b) compares the airfoil and flat-plate cases at $x/\theta_o = 0$. At very high frequencies f (i.e., 10 kHz), the PSD levels are slightly lower in the flat-plate case, but an overall match is observed for the majority of the frequency range. This suggests that any effect of the history of airfoil boundary layer prior to the flat-plate inlet location is minimal on the wall-pressure spectrum.

In Fig. 9(c), the PSDs are compared at $x/\theta_o = 290$. At this x location the β values are similar between the two cases (Fig. 7(b)). The PSD levels in both cases overlap in the low- and mid-frequency ranges. But for frequency higher than 7000 Hz, a faster drop of PSD level with increasing frequencies is observed for the flat-plate case. Thus the effect of convex curvature on wall-pressure PSD appears to be an augmentation of high-frequency contents.

At $x/\theta_o = 340$ near the trailing edge shown in Fig. 9(d), a faster drop in high-frequency levels with increasing frequency is again seen for the flat-plate case, for a wider range of frequencies starting from 4000 Hz. Such a difference in a wider range of the frequency spectrum than at upstream x locations is expected as the wall-pressure r.m.s. are significantly different, higher in the airfoil case, at this location (Fig. 9(a)). In addition, the spectrum in the airfoil case displays a local peak at high frequencies between 10 kHz and 20 kHz, which is likely acoustic and caused by the extra noise source in the airfoil wake as seen in the compressible DNS studies of Wu, Moreau, and Sandberg [54]. Such an acoustic hump at high frequency is not observed in the flat-plate case

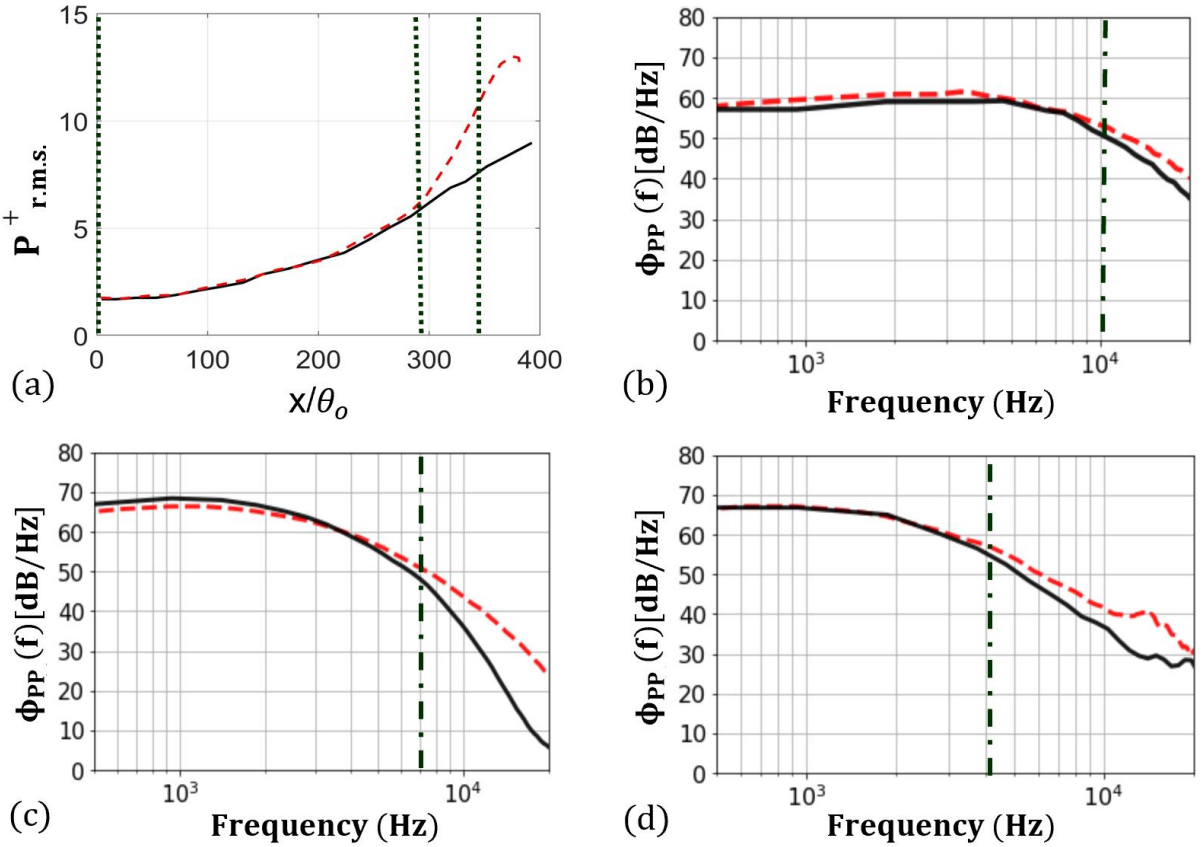

图 9. (a) Variation of r.m.s. wall-pressure fluctuations in airfoil (- - -) and flat-plate (———) cases. Vertical dotted lines indicate x locations used for comparison in (b,c,d), associated with sensors 7, 21, 24 on airfoil[53]. Power spectral density of wall-pressure fluctuations at (b) $x/\theta_o = 0$, (c) $x/\theta_o = 290$, and (d) $x/\theta_o = 340$. In (b-d), vertical lines indicate the frequency at which the difference between both cases is at around 5 percent.

for which an incompressible solver is used.

The spanwise coherence of wall-pressure fluctuations at each frequency can be quantified using the spanwise coherence function[67,68], γ^2, defined as:

$$\gamma^2(x, r_z; f) = \frac{|\Psi_{PP}(x, r_z; f)|^2}{\Phi_{PP}(x, f)^2}, \tag{4}$$

where Ψ_{PP} is the cross spectral density of wall-pressure fluctuations at any two spanwise locations at a given x:

$$\Psi_{PP}(x, r_z; f) = \frac{1}{2\pi} \left\langle \int_{-\infty}^{\infty} P'(x, 0, z, t) P'(x, 0, z + r_z, t + \tau) \exp(-\mathrm{i}2\pi f \tau) \mathrm{d}\tau \right\rangle, \tag{5}$$

τ is a time separation, and r_z is the spanwise separation between the two points.

Figure 10 compares the spanwise coherence of wall-pressure fluctuations at $x/\theta_o = 0$ and 290 on the airfoil. At $x/\theta_o = 0$ (Fig. 10(a,b)), the coherence distribution is approximately uniform at all frequency levels. This is seen for both flat-plate and airfoil cases. At $x/\theta_o = 290$ (Fig. 10(c,d)), the spanwise coherence is significantly widened at frequencies lower than 3000 Hz for both cases. This increase in coherence for wall-pressure statistics due to APG is consistent with previous observations of Na and Moin [14,15].

The spanwise coherence at two specific frequencies of 1500 Hz and 4500 Hz are quantitatively compared in Fig. 11 at the two x locations. For both cases, a faster decrease in coherence with a larger spanwise separation is

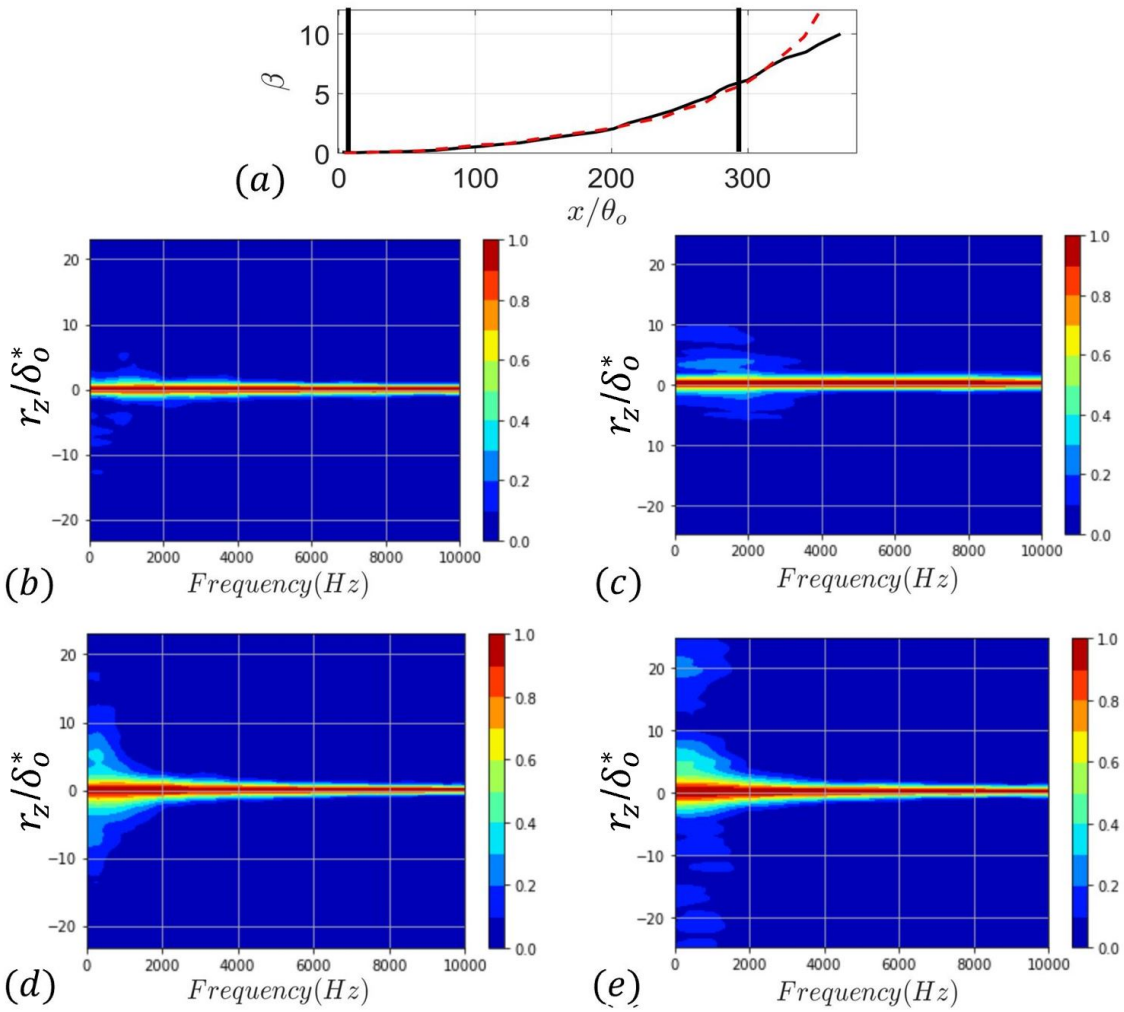

图 10. (a) Variation of Clauser parameter showing two x locations for comparison in (b-e). Spanwise coherence function for airfoil (b,d) and flat-plate (c,e) cases at $x/\theta_o = 0$ (b,c) and 290 (d,e).

observed for 1500 Hz than for 4500 Hz, at both x locations. This is consistent with the overall shorter spanwise coherence extent at the lower frequency as shown in Fig. 10. One difference between the two cases is the consistently shorter spanwise coherence for different frequencies in the airfoil case at the ZPG location of the airfoil ($x/\theta_o = 0$). This is thought to be an history effect of the upstream FPG in this case. Na and Moin [14,15] also observed that FPG leads to a decrease in wall-pressure correlations with spanwise separations. In addition, a shorter coherence is seen for the airfoil case than the flat-plate one for the lower frequency at $x/\theta_o = 290$. This could indicate that the convex wall curvature reduces the spanwise coherence of wall-pressure fluctuations at low frequencies. Another possible explanation is that the difference seen in the ZPG region is inherited by the flow and still present at this downstream location.

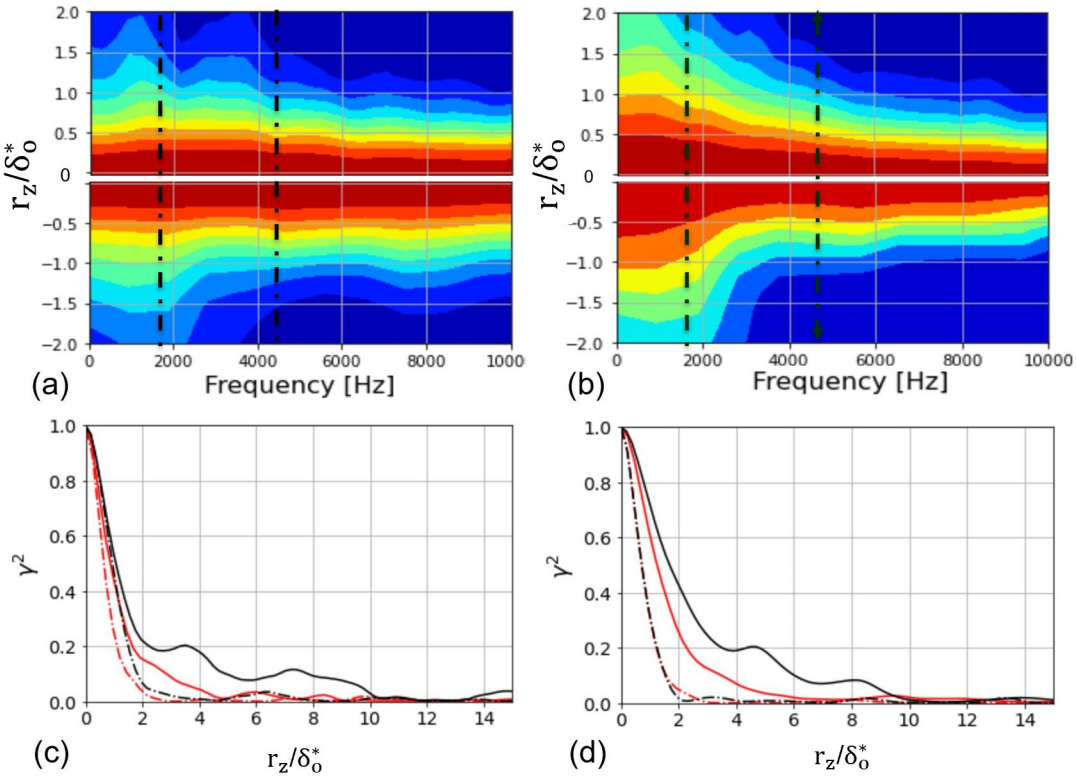

图 11. Zoomed-in plots showing spanwise coherence function at $x/\theta_o = 0$ (a) and 290 (b) in airfoil (top) and flat-plate (bottom) cases. Vertical lines indicate the frequencies (1500 Hz and 4500 Hz) at which the coherence function is plotted in (c,d). Variation of spanwise coherence function with spanwise separation at $x/\theta_o = 0$ (c) and 290 (d) for 1500 Hz (———) and 4500 Hz (– - –), in airfoil (red) and flat-plate (black) cases.

V. CONCLUSIONS

This study characterizes the effect of wall curvature in the presence of APG, in a setup designed to approximate typical flows on the suction side of a fan blade with a CD airfoil. To this end, flow statistics are compared between two DNS simulations of turbulent boundary layers over a flat plate and an airfoil with matching acceleration parameter, $K(x)$, in the ZPG to APG region of the boundary layer. At the "inlet" of the flat-plate simulation (located in the ZPG region of the boundary layer), the single-point statistics of velocity and wall pressure match well between the two cases. However, two-point statistics display quantitative differences in the extents of spatial coherences of velocity and wall pressure that are attributed to the history of upstream FPG flow in the airfoil case, absent in the flat-plate simulation.

As the boundary layer develops, the strength of pressure gradient relative to near-wall forces (measured by the Clauser parameter, β) and the strength of wall curvature (measured by δ/R) are both intensified. In the majority part of the boundary layer development, curvature effect on the flow appears to be masked by that of the APG. A few exceptions include the following. Far from the trailing edge (where the pressure gradient is relatively weak), the skin friction is lower in the airfoil case, consistent with the curvature effect observed in ZPG flows in the literature. In addition, near the trailing edge the outer-layer Reynolds stresses in the airfoil case is stronger than those in the flat-plate case, opposite from the expectation in a ZPG flow as found in past

studies. This suggests that, there, the APG effect (on augmenting outer-layer Reynolds stresses) is amplified and it dominates that of the curvature. Such an amplified APG effect in the airfoil case is consistent with the higher local β values than in the flat-plate case, suggesting that β is more appropriate than K as an indicator for the extent to which the turbulence statistics are affected by the mean pressure gradients. This higher β in the airfoil case may be attributed to the effect of curvature in reducing wall friction. As a result, one may conclude that in flows where pressure gradients are present the convex wall curvature indirectly augments the effect of pressure gradients on the boundary layer.

The statistical differences in wall-pressure fluctuations between the two cases are also quantified. The wall-pressure r.m.s. are more intense in the airfoil case approaching the trailing edge, which could be attributed to the higher β. In addition, the wall curvature appears to augment high-frequency fluctuations of the wall pressure. Thirdly, at the ZPG location the airfoil case gives more limited spanwise coherence of wall-pressure fluctuations at a wide range of frequencies due to the upstream FPG flow. Such a difference in coherence persists throughout the boundary layer development.

Other factors beside the wall curvature are also expected to contribute to the differences between the results of the two DNS simulations, mainly in the region close to the trailing edge. First, the lower wall friction and thicker boundary layer near the trailing edge in the airfoil case may also (at least partially) be attributed to trailing-edge effects[65], which are absent in the flat-plate simulation as the trailing edge is not simulated. In addition, the incompressible solver in the flat-plate simulation do not resolve acoustic fluctuations. This is probably the reason of the lack of a high-frequency hump in the wall-pressure spectra near the trailing edge, which is believed to originate from noise source in the airfoil wake[69].

The results demonstrate the modulation of APG effects on the flow by a convex wall. Overall, the boundary layer development, turbulence statistics and wall-pressure statistics are qualitatively similar with and without the wall curvature. This indicates that incompressible flat-plate boundary layer simulations similar to the present one can serve as low-cost surrogates of flows past an airfoil or other objects with mild curvatures to capture essential features of the developing boundary layer, for the purpose of turbulence and aeroacoustics models development. In other words, incompressible flat-plate boundary layers may be used to construct numerical databases used for modeling development, instead of using more expensive airfoil boundary layer simulations, as they reproduce key flow dynamics in a boundary layer developing on a curved airfoil blade.

ACKNOWLEDGMENTS

The authors gratefully acknowledge the support of Trane Technologies, Carrier, and Ziehl-Abegg under the Consortium of Ultra High-Efficiency and Quiet Fans. J.Y. also acknowledges support from the U.S. Office of Naval Research under the Basic Research Challenge program (Award No. N00014-17-1-2102). Computational support was supplied by Compute Canada and Michigan State University Institute for Cyber-Enabled Research.

DATA AVAILABILITY STATEMENT

The data that support the findings of this study are available from the corresponding author upon reasonable request.

REFERENCES

[1]G. Mellor and D. Gibson, "Equilibrium turbulent boundary layers," Journal of Fluid Mechanics **24**, 225–253 (1966).

[2]J. Yuan, J. Nicolle, U. Piomelli, and A. Giroux, "Modelling roughness and acceleration effects with application to the flow in a hydraulic turbine," in *IOP Conference Series: Earth and Environmental Science*, Vol. 22 (IOP Publishing, 2014) p. 022016.

[3]R. Balin and K. E. Jansen, "Direct numerical simulation of a turbulent boundary layer over a bump with strong pressure gradients," Journal of Fluid Mechanics **918** (2021).

[4]A. Jammalamadaka and H. Nagib, "Evaluation of turbulence models for boundary layers subjected to streamwise and spanwise pressure gradients," in *46th AIAA Aerospace Sciences Meeting and Exhibit* (2008) p. 643.

[5]H. Chen and V. Patel, "Near-wall turbulence models for complex flows including separation," AIAA journal **26**, 641–648 (1988).

[6]R. Shaheed, A. Mohammadian, and H. K. Gildeh, "A comparison of standard k–ε and realizable k–ε turbulence models in curved and confluent channels," Environmental Fluid Mechanics **19**, 543–568 (2019).

[7]A. Rezaeiha, H. Montazeri, and B. Blocken, "On the accuracy of turbulence models for CFD simulations of vertical axis wind turbines," Energy **180**, 838–857 (2019).

[8]F. H. Clauser, "Turbulent boundary layers in adverse pressure gradients," Journal of the Aeronautical Sciences **21**, 91–108 (1954).

[9]F. H. Clauser, "The turbulent boundary layer," in *Advances in applied mechanics*, Vol. 4 (Elsevier, 1956) pp. 1–51.

[10]A. Townsend, *The structure of turbulent shear flow* (Cambridge university press, 1980).

[11]R. L. Simpson, J. Strickland, and P. Barr, "Features of a separating turbulent boundary layer in the vicinity of separation," Journal of Fluid Mechanics **79**, 553–594 (1977).

[12]Z. Harun, J. P. Monty, R. Mathis, and I. Marusic, "Pressure gradient effects on the large-scale structure of turbulent boundary layers," Journal of Fluid Mechanics **715**, 477–498 (2013).

[13]P. R. Spalart and J. H. Watmuff, "Experimental and numerical study of a turbulent boundary layer with pressure gradients," Journal of Fluid Mechanics **249**, 337–371 (1993).

[14]Y. Na and P. Moin, "Direct numerical simulation of a separated turbulent boundary layer," Journal of Fluid Mechanics **374**, 379–405 (1998).

[15]Y. Na and P. Moin, "The structure of wall-pressure fluctuations in turbulent boundary layers with adverse pressure gradient and separation," Journal of Fluid Mechanics **377**, 347–373 (1998).

[16]A. G. Gungor, M. P. Simens, and J. Jiménez, "Direct numerical simulations of wake-perturbed separated boundary layers," Journal of Turbomachinery **134**, 061024:1–9 (2012).

[17]V. Kitsios, C. Atkinson, J. A. Sillero, G. Borrell, A. G. Gungor, J. Jiménez, and J. Soria, "Direct numerical simulation of a self-similar adverse pressure gradient turbulent boundary layer," International Journal of Heat and Fluid Flow **61**, 129–136 (2016).

[18]V. Kitsios, A. Sekimoto, C. Atkinson, J. A. Sillero, G. Borrell, A. G. Gungor, J. Jiménez, and J. Soria, "Direct numerical simulation of a self-similar adverse pressure gradient turbulent boundary layer at the verge of separation," Journal of Fluid Mechanics **829**, 392–419 (2017).

[19]C. D. Aubertine and J. K. Eaton, "Turbulence development in a non-equilibrium turbulent boundary layer with mild adverse pressure gradient," Journal of Fluid Mechanics **532**, 345–364 (2005).

[20]A. Bobke, R. Vinuesa, R. Örlü, and P. Schlatter, "History effects and near equilibrium in adverse-pressure-gradient turbulent boundary layers," Journal of Fluid Mechanics **820**, 667–692 (2017).

[21]R. J. Volino, "Non-equilibrium development in turbulent boundary layers with changing pressure gradients," Journal of Fluid Mechanics **897** (2020).

[22]J. P. Monty, Z. Harun, and I. Marusic, "A parametric study of adverse pressure gradient turbulent boundary layers," International Journal of Heat and Fluid Flow **32**, 575–585 (2011).

[23]C. S. Vila, R. Örlü, R. Vinuesa, P. Schlatter, A. Ianiro, and S. Discetti, "Adverse-pressure-gradient effects on turbulent boundary layers: statistics and flow-field organization," Flow, turbulence and combustion **99**, 589–612 (2017).

[24]R. Vinuesa, R. Örlü, C. S. Vila, A. Ianiro, S. Discetti, and P. Schlatter, "Revisiting history effects in adverse-pressure-gradient turbulent boundary layers," Flow, turbulence and combustion **99**, 565–587 (2017).

[25]M. Bross, T. Fuchs, and C. J. Kähler, "Interaction of coherent flow structures in adverse pressure gradient turbulent boundary layers," Journal of Fluid Mechanics **873**, 287–321 (2019).

[26]R. Vinuesa, P. S. Negi, M. Atzori, A. Hanifi, D. S. Henningson, and P. Schlatter, "Turbulent boundary layers around wing sections up to $\mathrm{Re}_c = 1,000,000$," International Journal of Heat and Fluid Flow **72**, 86–99 (2018).

[27]J.-H. Lee and H. J. Sung, "Structures in turbulent boundary layers subjected to adverse pressure gradients," Journal of Fluid Mechanics **639**, 101–131 (2009).

[28]S. M. Hosseini, R. Vinuesa, P. Schlatter, A. Hanifi, and D. S. Henningson, "Direct numerical simulation of the flow around a wing section at moderate Reynolds number," International Journal of Heat and Fluid Flow **61**, 117–128 (2016).

[29]R. Vinuesa, S. M. Hosseini, A. Hanifi, D. S. Henningson, and P. Schlatter, "Pressure-gradient turbulent boundary layers developing around a wing section," Flow, turbulence and combustion **99**, 613–641 (2017).

[30]P. Bradshaw, "The analogy between streamline curvature and buoyancy in turbulent shear flow," Journal of Fluid Mechanics **36**, 177–191 (1969).

[31]P. Bradshaw, "Effects of streamline curvature on turbulent flow," Tech. Rep. (AGARD Paris (France), 1973).

[32]B. Ramaprian and B. Shivaprasad, "The structure of turbulent boundary layers along mildly curved surfaces," Journal of Fluid Mechanics **85**, 273–303 (1978).

[33]M. Gibson, C. Verriopoulos, and N. Vlachos, "Turbulent boundary layer on a mildly curved convex surface," Experiments in Fluids **2**, 17–24 (1984).

[34]J. C. Gillis and J. P. Johnston, "Turbulent boundary-layer flow and structure on a convex wall and its redevelopment on a flat wall," Journal of Fluid Mechanics **135**, 123–153 (1983).

[35]K. Muck, P. Hoffmann, and P. Bradshaw, "The effect of convex surface curvature on turbulent boundary layers," Journal of Fluid Mechanics **161**, 347–369 (1985).

[36]R. M. So and G. L. Mellor, "Experiment on convex curvature effects in turbulent boundary layers," Journal of Fluid Mechanics **60**, 43–62 (1973).

[37]A. C. Schwarz and M. W. Plesniak, "The influence of interacting strain rates on turbulence in convex boundary layers," Physics of Fluids **8**, 3163–3171 (1996).

[38]V. Patel and F. Sotiropoulos, "Longitudinal curvature effects in turbulent boundary layers," Progress in Aerospace Sciences **33**, 1–70 (1997).

[39]E. Tulapurkara, A. Khoshnevis, and J. Narasimhan, "Wake-boundary layer interaction subject to convex and concave curvatures and adverse pressure gradient," Experiments in fluids **31**, 697–707 (2001).

[40]L. Ding, T. Saxton-Fox, M. Hultmark, and A. Smits, "Effects of pressure gradients and streamline curvature on the statistics of a turbulent pipe flow," in *11^{th} International Symposium on Turbulence and Shear Flow Phenomena (TSFP)* (2019).

[41]G. Brethouwer, "Turbulent flow in curved channels," Journal of Fluid Mechanics **931** (2022).

[42]S. Moreau and M. Sanjosé, "Sub-harmonic broadband humps and tip noise in low-speed ring fans," Journal of the Acoustical Society of America **139**, 118–127 (2016).

[43]M. Sanjosé and S. Moreau, "Fast and accurate analytical modeling of broadband noise for a low-speed fan," Journal of the Acoustical Society of America **143**, 3103–3113 (2018).

[44]R. K. Amiet, "Noise due to turbulent flow past a trailing edge," Journal of Sound and Vibration **47**, 387–393 (1976).

[45]M. Roger and S. Moreau, "Back-scattering correction and further extensions of Amiet's trailing edge noise model. Part 1: theory," Journal of Sound and Vibration **286**, 477–506 (2005).

[46]S. Moreau and M. Roger, "Back-scattering correction and further extensions of Amiet's trailing-edge noise model. Part II: Application," Journal of Sound and Vibration **323**, 397–425 (2009).

[47]Y. Rozenberg, G. Robert, and S. Moreau, "Wall-pressure spectral model including the adverse pressure gradient effects," AIAA journal **50**, 2168–2179 (2012).

[48]S. Lee, "Empirical wall-pressure spectral modeling for zero and adverse pressure gradient flows," AIAA Journal **56**, 1818–1829 (2018).

[49]M. R. Catlett, J. Forest, J. M. Anderson, and D. Stewart, "Empirical spectral model of surface pressure fluctuations beneath adverse pressure gradients," in *20th AIAA/CEAS Aeroacoustics Conference* (2014) p. 2910.

[50]N. Hu, "Empirical model of wall pressure spectra in adverse pressure gradients," AIAA Journal **56**, 3491–3506 (2018).

[51]G. Grasso, P. Jaiswal, H. Wu, S. Moreau, and M. Roger, "Analytical models of the wall-pressure spectrum under a turbulent boundary layer with adverse pressure gradient," Journal of Fluid Mechanics **877**, 1007–1062 (2019).

[52]P. Jaiswal, S. Moreau, F. Avallone, D. Ragni, and S. Pröbsting, "On the use of two-point velocity correlation in wall-pressure models for turbulent flow past a trailing edge under adverse pressure gradient," Physics of Fluids **32**, 105105 (2020).

[53]H. Wu, S. Moreau, and R. Sandberg, "Effects of pressure gradient on the evolution of velocity-gradient tensor invariant dynamics on a controlled-diffusion aerofoil at $\mathrm{Re}_c = 150,000$," Journal of Fluid Mechanics **868**, 584–610 (2019).

[54]H. Wu, S. Moreau, and R. Sandberg, "On the noise generated by a controlled-diffusion aerofoil at $Re_c = 1.5 \times 10^5$," Journal of Sound and Vibration **506**, 116152: 1–20 (2020).

[55]A. Keating, U. Piomelli, K. Bremhorst, and S. Nešić, "Large-eddy simulation of heat transfer downstream of a backward-facing step," Journal of Turbulence **5**, 020 (2004).

[56]J. Yuan and U. Piomelli, "Numerical simulation of a spatially developing accelerating boundary layer over roughness," Journal of Fluid Mechanics **780**, 192–214 (2015).

[57]T. S. Lund, X. Wu, and K. D. Squires, "Generation of turbulent inflow data for spatially-developing boundary layer simulations," Journal of Computational Physics **140**, 233–258 (1998).

[58]I. Orlanski, "A simple boundary condition for unbounded hyperbolic flows," Journal of Computational Physics **21**, 251–269 (1976).

[59]K. P. Griffin, L. Fu, and P. Moin, "General method for determining the boundary layer thickness in nonequilibrium flows," Physical Review Fluids **6**, 024608 (2021).

[60]P. Schlatter and R. Örlü, "Assessment of direct numerical simulation data of turbulent boundary layers," Journal of Fluid Mechanics **659**, 116–126 (2010).

[61]P. R. Spalart, "Direct simulation of a turbulent boundary layer up to Re_θ= 1410," Journal of Fluid Mechanics **187**, 61–98 (1988).

[62]C. Bourassa and F. O. Thomas, "An experimental investigation of a highly accelerated turbulent boundary layer," Journal of Fluid Mechanics **634**, 359–404 (2009).

[63]U. Piomelli and J. Yuan, "Numerical simulations of spatially developing, accelerating boundary layers," Phys. Fluids **25**, 101304–1—21 (2013).

[64]J. A. Sillero, J. Jiménez, and R. D. Moser, "Two-point statistics for turbulent boundary layers and channels at Reynolds numbers up to $\delta^+ \approx 2000$," Physics of Fluids **26**, 105109 (2014).

[65]A. Messiter, "Boundary-layer flow near the trailing edge of a flat plate," SIAM Journal on Applied Mathematics **18**, 241–257 (1970).

[66]E. Cohen and X. Gloerfelt, "Influence of pressure gradients on wall pressure beneath a turbulent boundary layer," Journal of Fluid Mechanics **838**, 715–758 (2018).

[67]É. Salze, C. Bailly, O. Marsden, E. Jondeau, and D. Juvé, "An experimental characterisation of wall pressure wavevector-frequency spectra in the presence of pressure gradients," in *20^{th} AIAA/CEAS Aeroacoustics Conference* (2014) p. 2909.

[68]G. Corcos, "Resolution of pressure in turbulence," The Journal of the Acoustical Society of America **35**, 192–199 (1963).

[69]H. Wu, S. Moreau, and R. D. Sandberg, "On the noise generated by a controlled-diffusion aerofoil at rec= 1.5$\times$ 105," Journal of Sound and Vibration **487**, 115620 (2020).